The Radical Cation of *syn*-Tricyclooctadiene and Its Rearrangement Products

Thomas Bally,*[a] Stefan Bernhard,[a] Stephan Matzinger,[a] Jean-Luc Roulin,[a] G. Narahari Sastry,[a] Leo Truttmann,[a] Zhendong Zhu,[a] Andrzej Marcinek,*[b] Jan Adamus,[b] Rafal Kaminski,[b] Jerzy Gebicki,*[b] Ffrancon Williams,*[c] Guo-Fei Chen,[c] and Markus P. Fülscher[d]

Abstract: The *syn* dimer of cyclobutadiene (tricyclo[4.2.0.$0^{2,5}$]octa-3,7-diene, **TOD**) is subjected to ionization under different conditions and the resulting species are probed by optical and ESR spectroscopy. By means of quantum chemical modelling of the potential energy surfaces and the optical spectra, it is possible to assign the different products that arise spontaneously after ionization or after subsequent warming or illumination of the samples. Based on these findings, we propose a mechanistic scheme which involves a partitioning of the incipient radical cation of **TOD** between two electronic states. These two states engage in (near) activationless decay to the more stable valence isomers, cyclooctatetraene (**COT**$^{\bullet+}$) and a bis-cyclobutenylium radical cation **BCB**$^{\bullet+}$. The latter product undergoes further rearrangement, first to tetracyclo[4.2.0.$0^{2,4}$.$0^{3,5}$]oct-7-ene (**TCO**$^{\bullet+}$) and eventually to bicyclo[4.2.0]octa-2,4,7-triene (**BOT**$^{\bullet+}$) which can also be generated photochemically from **BCB**$^{\bullet+}$ or **TCO**$^{\bullet+}$. The surprising departure of *syn*-**TOD**$^{\bullet+}$ from the least-motion reaction path leading to **BOT**$^{\bullet+}$ can be traced to strong vibronic interactions (second-order Jahn-Teller effects) which prevail in both possible ground states of *syn*-**TOD**$^{\bullet+}$. Such effects seem to be more important in determining the intramolecular reactivity of radical cations than orbital or state symmetry rules.

Keywords: electronic structure · radical ions · rearrangements · spectroscopy · theoretical calculations

Introduction

$(CH)_8$ hydrocarbons show a very rich and often surprising thermal and photoinduced chemistry.[1] The same is true of their radical cations, e. g., those which stood at the focus of earlier investigations by the Fribourg and Knoxville groups.[2–5] In the preceding paper[6] we investigated the fate of another interesting $(CH)_8$ isomer, the *anti* dimer of cyclobutadiene (tricyclo[4.2.0.$0^{2,5}$]octa-3,7-diene (**TOD**), see Scheme 1) on ionization under various conditions. Thereby, *anti*-**TOD**$^{\bullet+}$ was found to partition between two products, one of which is the radical cation of the expected valence isomer, bicyclo[4.2.0]octa-2,4,7-triene (**BOT**$^{\bullet+}$). The other product results from a cascade of reactions involving an unprecedented type of valence isomerization and two hydrogen atom

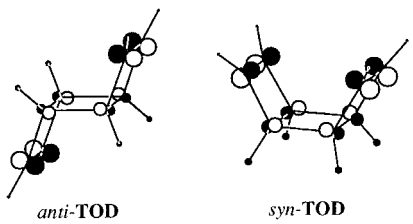

Scheme 1. MO representation of *anti*-**TOD** and *syn*-**TOD**.

[a] Prof. T. Bally, Dr. S. Bernhard,[+] Dr. S. Matzinger, J.-L. Roulin, Dr. G. N. Sastry, Dr. L. Truttmann, Dr. Z. Zhu
Institut de Chimie Physique
Université de Fribourg, Pérolles
1700 Fribourg (Switzerland)
Fax: (+41) 26-300-9737
E-mail: Thomas.Bally@unifr.ch

[b] Dr. A. Marcinek, Prof. J. Gebicki, Dr. J. Adamus, Dr. R. Kaminski[++]
Institute of Applied Radiation Chemistry
Technical University of Lodz
90-924 Lodz (Poland)
Fax: (+48) 42-636 5008
E-mail: marcinek@ck-sg.p.lodz.pl

[c] Prof. F. Williams, Dr. G.-F. Chen
Department of Chemistry, University of Tennessee
Knoxville, TN 37996-1600 (USA)
Fax: (+1) 865-974-3454
E-mail: ffwilliams@utk.edu

[d] Dr. M. P. Fülscher
Department of Theoretical Chemistry, Chemical Centre
22100 Lund (Sweden)
E-mail: markus@signe.teokem.lu.se

[+] Current address:
Department of Chemistry and Chemical Biology, Cornell University
Ithaca, NY 14853-1301 (USA)

[++] on leave from CBMM, Polish Academy of Sciences 90-963 Lodz (Poland)

Supporting information for this article is available on the www under http://www.wiley-vch.de/home/chemistry/ or from the author.

0947-6539/00/0605-0858 $ 17.50+.50/0 *Chem. Eur. J.* **2000**, *6*, No. 5

shifts which eventually lead to the previously identified radical cation of 1,4-dihydropentalene.[3] Especially this second, surprising result led us to subject also the *syn* isomer of **TOD** to the same experiments.

The ground states of the radical cations of both **TOD** isomers have a very similar electronic structure as judged by the shape of their singly occupied MOs. These result in both cases from the antibonding interaction between the symmetric combination of olefinic π-MOs and the appropriate σ_{CC} bonding MO of the central four-membered ring (see Scheme 1), that is the interaction which accounts for the "through-bond" component of the splitting of the π-MOs in **TOD**.[7] One would therefore expect the two isomers to show a similar reactivity, in particular with regard to their decay to **BOT**$^{\bullet+}$ (the reaction leading to the dihydropentalene cannot occur in an analogous fashion in *syn*-**TOD**$^{\bullet+}$ for steric reasons).

However, as will be shown below, this expectation was not fulfilled in that *syn*-**TOD**$^{\bullet+}$ follows entirely different rearrangement pathways. The only analogy between the two isomers is that both undergo a partitioning into two reaction channels, although, in contrast to the case of *anti*-**TOD**, this partitioning is not due to a bifurcation in the potential energy surface but to two different electronic states which may be populated on ionization of *syn*-**TOD**. We will try to show that the divergence in the chemistry of the two isomers is a result of the operation of strong vibronic interactions which lead *syn*-**TOD**$^{\bullet+}$ into different directions than its *anti* counterpart.

Results and Discussion

Ionization of *syn*-TOD: Trace a) in Figure 1 shows the spectrum that is obtained upon pulse radiolysis of *syn*-**TOD** in MCH/BuCl at 30 K, whereas spectra b) and c) illustrate the result of subsequent thermal relaxation at 75 K. These spectra clearly demonstrate the thermal conversion of a species **A** responsible for the strong 545 nm band to a secondary product **B** with a much weaker, broad band centered around 820 nm. After prolonged annealing of the matrix at 90 K, spectrum d) is obtained which consists of a broad band with a maximum at 505 nm with a shoulder at 650 nm and a sharper component at 400 nm.

The 505 nm band is undoubtedly due to the radical cation of cyclooctatetraene (**COT**$^{\bullet+}$) whose authentic spectrum is shown with a dashed line. There is reason to assume that **COT**$^{\bullet+}$ is not formed as a result of the annealing, but is present from the outset, leading to the shoulder at ≈480 nm in spectra a)–c). On the other hand, a 400 nm band, which is clearly not present after radiolysis, arises as a shoulder during annealing. Figure 2 shows the latter stages of this process in more detail, which reveals that species **B** is also thermally labile at 90 K and that probably this species serves as the direct precursor of the carrier of the 400 nm band which we provisionally assign to a product **C**.

The insert to Figure 1 indicates that species **A** is formed beyond the time resolution of our detection systems (microseconds), even at 10 K which suggests that it is the parent radical cation of *syn*-**TOD**, a hypothesis which we will

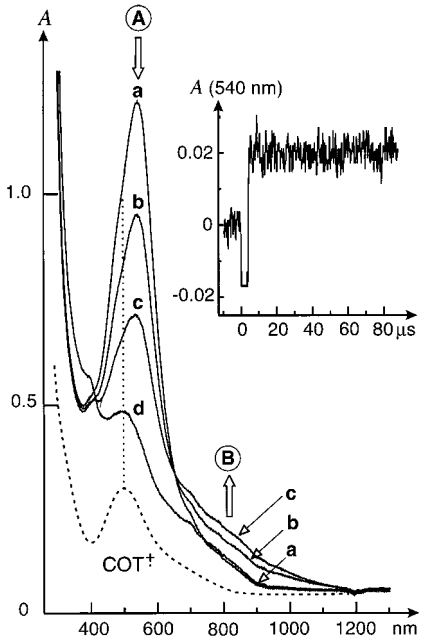

Figure 1. EA spectra obtained after pulse radiolysis (10 pulses, dose ≈10 kGy) of *syn*-**TOD** (0.01M) in a MCH/BuCl glass at 30 K. Spectrum a): initially at 30 K. Spectra b) and c): after thermal relaxation of the matrix at 75 K for 65 and 215 min, respectively. Spectrum d): after prolonged annealing of the matrix at 90 K. Dashed line represents spectrum obtained on ionization of **COT**. Inset: formation of the 545 nm absorption signal at 10 K (2 µs electron pulse, dose 0.5 kGy).

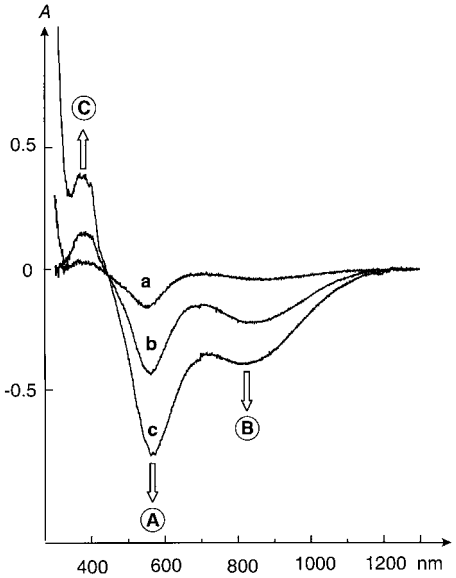

Figure 2. Difference spectra observed on thermal relaxation of the matrix (see Figure 1 for details) at 90 K for a) 10 min, b) 30 min and c) 60 min.

examine below. The thermal decay of **A** was found to follow dispersive kinetics, as it is typical for thermal rearrangements in solid media: A plot of ln A versus t^{α} leads to a straight line for $\alpha = 0.48$ (Figure 3) which indicates that the rate constant varies with time according to $k = B \cdot t^{\alpha-1}$.[8, 9] A mean lifetime τ_0 of 689 s can be extracted from this result, but we should caution that this is burdened with some error because the fastest part of the process (between the end of the radiolysis and the beginning of the measurements) is not accounted for.

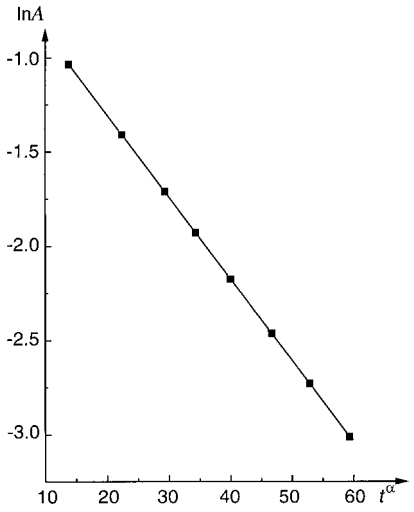

Figure 3. Dispersive kinetics of the thermal decay of the 545 nm absorption band at 77 K. The t^{α} scale of the abscissa refers to t in seconds with $\alpha = 0.48$.

Finally, we note that species **A** can also be bleached photochemically to yield **C** ($\lambda_{max} = 400$ nm) by irradiation at 30 K through a 500 nm interference filter, as shown in Figure 4.

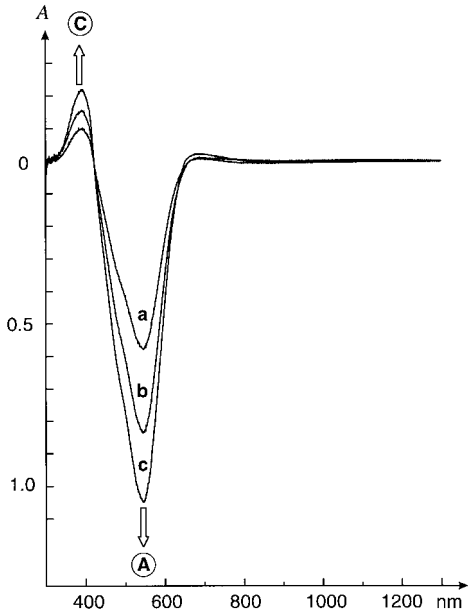

Figure 4. Difference spectra for the photolysis of an MCH/BuCl (30 K) solution of ionized *syn*-**TOD** at 500 nm (400 W xenon lamp) for a) 4 min, b) 20 min and c) 35 min.

Ionization of *syn*-**TOD** in Freon matrices (F-11/F-114B2) by γ-irradiation at 77 K results in spectrum a) in Figure 5. Obviously, the facile thermal **A** $\rightarrow$**B** rearrangement is complete by the time this spectrum is recorded, but we note again in this experiment that $\mathbf{COT}^{\bullet+}$ is formed concomitantly with intermediate **B** whose spectrum can be obtained by subtraction of $\mathbf{COT}^{\bullet+}$ (dashed line). Photolysis at >820 nm leads to the disappearance of **B** and the appearance of the 400 nm band of **C**. Subtraction of $\mathbf{COT}^{\bullet+}$ (whose concentration does not seem to have increased in this conversion) reveals that, next to the 400 nm band, **C** has a shoulder at 500 nm (dashed line).

This spectrum is reminiscent of that of the radical cation of bicyclo[4.2.0]octa-2,4-diene,[10] which suggests that **C** is the radical cation of the related C_8H_8 compound, bicyclo[4.2.0]octa-2,4,7-triene ($\mathbf{BOT}^{\bullet+}$) that had already been found and identified upon oxidation of *anti*-**TOD**.[6] In addition to the typical pair of "diene cation" bands at 400 and 500 nm,[11] $\mathbf{BOT}^{\bullet+}$ is expected to show an electronic transition involving transfer of an electron from the olefin to the diene moiety. The energy of this transition can be estimated from the difference in ionization potentials of cyclobutene and cyclohexadiene (9.43 – 8.25 eV)[12] which on a wavelength scale corresponds to a band around 1000 nm. However, as a result of the weak interaction between the two moieties, the transition moment is expected to be very weak so it is not surprising that this band escapes detection in our experiment. However, its presence can be proven by photolysis at >600 nm, that is outside the range of the observed absorptions, which leads to slow conversion to $\mathbf{COT}^{\bullet+}$ (cf. spectrum 5c).

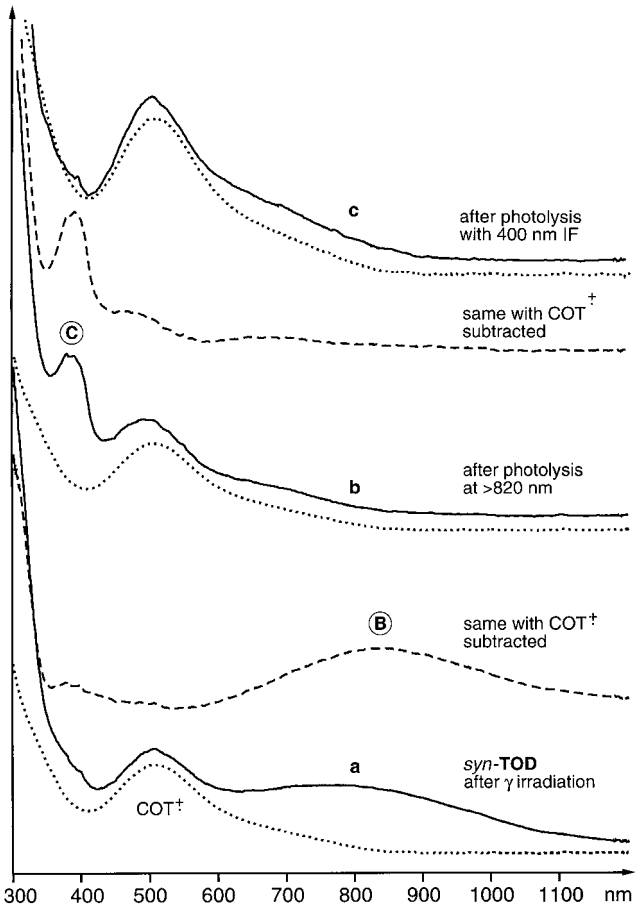

Figure 5. Electronic absorption spectra obtained after γ-irrradiation of *syn*-**TOD** in the Freon mixture at 77 K a). Dotted line represents spectrum obtained on ionization of **COT** under the same conditions, dashed line shows the result of subtracting this from spectrum a). After photolysis at >820 nm, spectrum b) is obtained (again the dashed line shows the result of subtracting the dotted spectrum of ionized **COT** from that), whereas photolysis at 400 nm converts this into spectrum c).

0947-6539/00/0605-0860 $ 17.50+.50/0 *Chem. Eur. J.* **2000**, *6*, No. 5

Finally, we followed the above conversions by ESR spectroscopy. The spectrum obtained on radiolysis of *syn*-**TOD** in F-113 consists of signals from the bicyclo[3.3.0]octa-2,6-diene-4,8-diyl radical cation (**BOD**$^{\bullet+}$)[13] that are clearly recognizable from the well-resolved 1:4:6:4:1 quintet substructures in the wings (Figure 6a). It is also evident that there are additional strong signals in the center which greatly distort the center lines of **BOD**$^{\bullet+}$ but no definite hyperfine pattern can be discerned for these extra features. However, the strong center line is indicative of a singlet component arising from some **COT**$^{\bullet+}$ formation.[4, 14] After illumination of the sample with NIR light ($\lambda > 840$ nm), the spectrum of Figure 6b) shows that a new group of 17 resolved components represented within the vertical bars have grown in strongly, and this pattern displays the characteristic fine structure of the complete 23-line ESR spectrum of **BOT**$^{\bullet+}$ (cf. Figure 1 in the accompanying paper.[6]) In contrast, the NIR photobleaching produces little or no change in the intensity of the **BOD**$^{\bullet+}$ signal.

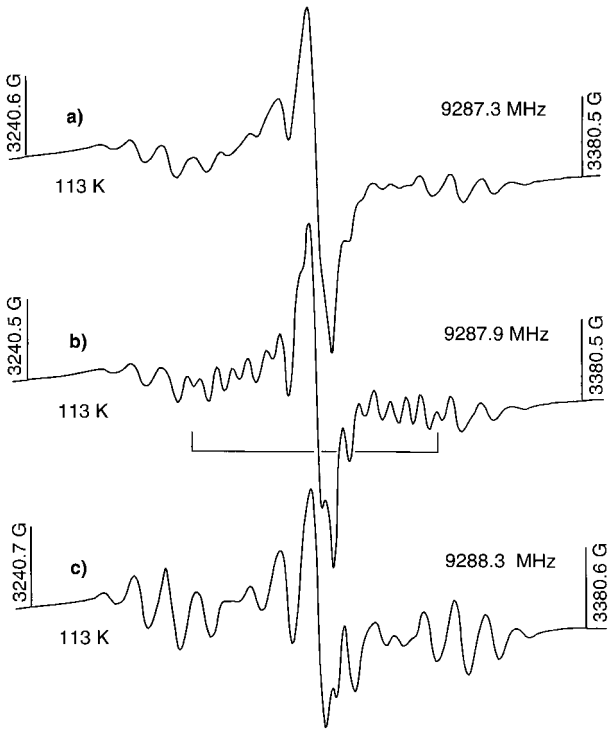

Figure 6. First-derivative ESR spectra showing a) the initial spectrum obtained after radiolytic oxidation at 77 K of a dilute solution of *syn*-**TOD** in F-113, and b) the spectrum recorded after illumination of the sample with near-infrared (NIR) light ($\lambda > 840$ nm). The sharp lines of the NIR-induced signals indicated within the vertical bars and extending through the central region of spectrum b) are assigned to **BOT**$^{\bullet+}$ (see text). Spectrum c) was recorded after a subsequent illumination in the wideband 340–580 nm region which converts all the **BOT**$^{\bullet+}$ in b) to additional **BOD**$^{\bullet+}$ in c). The spectra were recorded with identical spectrometer settings.

A further exposure of the F-113 sample (Figure 6b) to wideband 340–580 nm illumination converted **BOT**$^{\bullet+}$ to the clean spectrum of **BOD**$^{\bullet+}$ shown in Figure 6c. From this significant increase in the **BOD**$^{\bullet+}$ signal, it can be estimated that the ratio of **BOT**$^{\bullet+}$ to **BOD**$^{\bullet+}$ in Figure 6b is about 1.5. In view of the strong matrix effect on the products of radiolytic oxidation of *anti*-**TOD**,[6] it was also of interest to carry out a study of *syn*-**TOD** oxidation in the F-114B2 matrix. The spectra obtained in this medium are much more poorly resolved, but they also clearly reveal the presence of **BOT**$^{\bullet+}$ after NIR bleaching. Hence the ionization of *syn*-**TOD** produces much more convergent results in different media than that of its *anti* isomer.

Assignment of the primary product A: As mentioned above, the immediate appearance of the strong 545 nm band of **A** on ionization suggests its assignment to the parent radical cation of *syn*-**TOD**. A theoretical confirmation of this assignment is not so straightforward because it is not clear a priori what is the nature of the ground state of **TOD**$^{\bullet+}$. The nature of this problem becomes evident from the photoelectron (PE) spectrum which we have remeasured and which is reproduced in Figure 7.

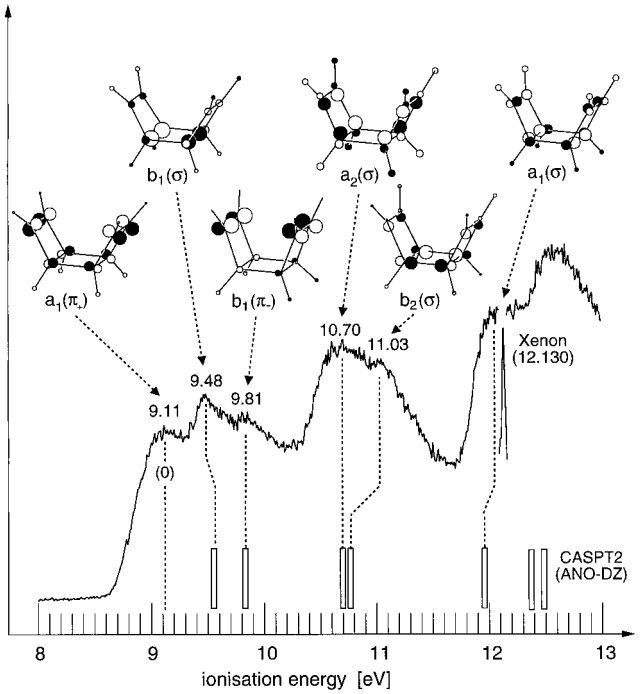

Figure 7. Photoelectron (PE) spectrum of *syn*-**TOD**. White bars denote excited state energies obtained from CASPT2-calculations at the geometry of neutral **TOD**, relative to the maximum of the first PE band (dashed line at (0)). Molecular orbitals from SCF/6–31G* calculations on neutral *syn*-**TOD**.

The ordering of the highest orbitals (or the lowest radical cation states) in *syn*-**TOD**, which results from a delicate balance of through-space and through-bond interaction between the two π-system, has been a matter of some debate.[15–18] This was finally settled in favor of $a_1(\pi_+)$ below $b_1(\sigma)$ below $b_1(\pi_-)$.[7, 18] Our CASPT2 calculations of **TOD**$^{\bullet+}$ at the equilibrium geometry of neutral **TOD** (Table 1) and white bars in Figure 7) are generally in good agreement with the observed PE band positions, also for higher states, which instills some confidence in this method to predict excited state energies in **TOD**$^{\bullet+}$. Interestingly, the CASSCF results show that—at the neutral geometry which is the relevant one in the

Table 1. Results of CASPT2 calculations for *syn*-**TOD**$^{\bullet+}$ at the geometry of the neutral.[a]

State	PES/ eV[b]	CASPT2/ eV[c]	% K[d]
1^2A_1	(0)	(0)	93
1^2B_1	0.37	0.44	93
2^2B_1	0.70	0.71	91
1^2A_2	1.59	1.59	90
1^2B_2	1.92	1.64	90
2^2A_1	2.95	2.85	89

[a] Geometry optimized by B3LYP/6–31G*; [b] peak positions relative to first peak in PE spectrum (cf. Figure 7); [c] active space in CASSCF calculations: 15 electrons in 10 orbitals; details of the calculations are given in the Supporting Information; [d] percent Koopmans' character: summed contributions of single-hole configurations (proportional to intensity of PE band).

discussion of the PE spectrum—any attempt to assign shoulders in the first, broad PE band to the $b_1(\sigma)$ and the $b_1(\pi_-)$ MO may be futile, because the two $^2B_1$ states which are predicted above the $^2A_1$ ground state are composed of strongly mixed configurations resulting from electron ejection out of both high-lying b_1 MOs.

The proximity of the first three states indicates that any of them could possibly become the most stable state of **TOD**$^{\bullet+}$ after relaxation to the radical cation geometry. Thus, we had to subject each of the three states to individual B3LYP geometry optimizations whose results are represented in Figure 8.[19] The changes in the two important parameters, the folding angle ω and the bond length R, are in accord with expectations on the basis of the nodal structure of the MOs from which ionization occurs in each of the three states. According to B3LYP, the ordering of stabilities is $^2A_1(\pi_+)$ 3.4 kcal mol^{-1} below $^2B_1(\sigma)$ and 9.1 kcal mol^{-1} below $^2B_1(\pi_-)$. In contrast, CCSD(T) single point calculations at the B3LYP geometries predict the $^2B_1(\sigma)$ state to be the most stable one, 1.95 kcal mol^{-1} below $^2A_1(\pi_+)$, and 9.4 kcal mol^{-1} below $^2B_1(\pi_-)$. Thus, we can make no definitive statements on the ordering of stabilities of the $^2B_1$ and the $^2A_1$ states after relaxation. However, they are competitive in energy and it cannot be excluded that *syn*-**TOD** partitions between these two "electromers" after vertical ionization. Therefore both states have to be considered as possible candidates for the ground state of *syn*-**TOD**$^{\bullet+}$.

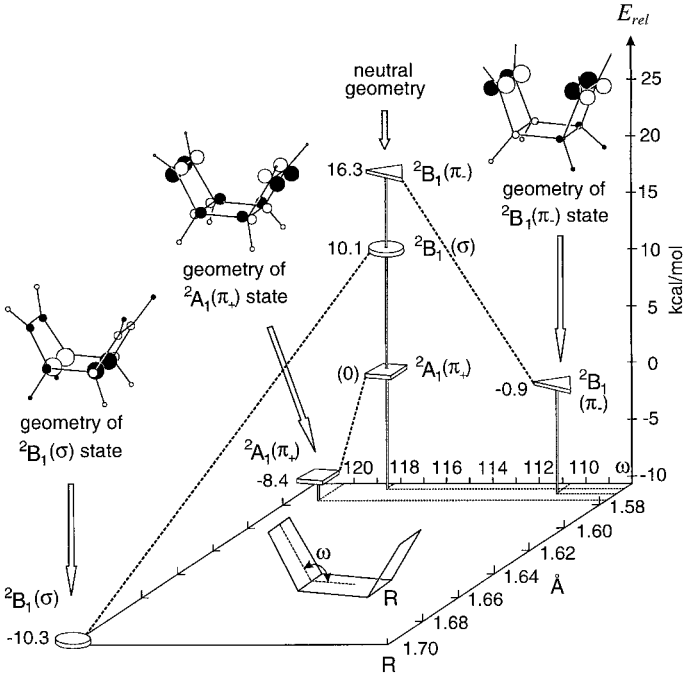

Figure 8. Diagram showing the relaxation of vertically formed *syn*-**TOD**$^{\bullet+}$ ($\Rightarrow$ neutral geometry) in the three different states indicated above each column (pictures denote singly occupied MO in each state). Geometries are from B3LYP/6–31G*, relative ground-state energies from RCCSD(T)/cc-pVDZ, excited state energies at the neutral geometry from CASPT2/ANO-DZP calculations.

According to second-derivative calculations, the two π-states ($^2A_1$ and the $^2B_1$) are minima on the B3LYP/6–31G* surface, whereas the $^2B_1(\sigma)$ state is a saddle point representing the transition state for the interconversion of two structures of C_s symmetry where spin and charge are localized mostly in one of the C–C bonds that are shared by two four-membered rings.[20, 21] Although this distortion is rather pronounced (the two affected C–C bond lengths differ by 0.34 Å), it is accompanied by a gain of only 0.67 kcal mol^{-1}, and single-point CCSD(T) calculations at the B3LYP geometries predict the localized C_s structure to lie 0.53 kcal mol^{-1} above the delocalized one. This indicates an extreme flatness of the surface for distortion of the $^2B_1(\sigma)$ state, and we therefore need to consider both C_{2v} and C_s structures in the subsequent calculations of excited states of *syn*-**TOD**$^{\bullet+}$.

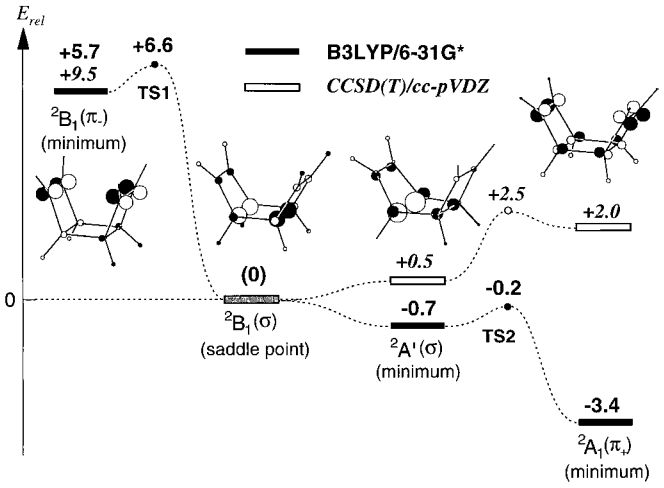

Figure 9. Diagram showing the interconversions of the different states of *syn*-**TOD**$^{\bullet+}$. Solid bars and bold numbers are from B3LYP/6–31G* calculations, open bars and italic numbers from single-point CCSD(T)/cc-pVDZ calculations at B3LYP geometries. All energies are relative to that of the $^2B_1(\sigma)$ state of *syn*-**TOD**$^{\bullet+}$ in C_{2v} symmetry.

States of the same symmetry often undergo facile interconversion in radical ions. Thus, we were not surprised to find a very low-lying transition state for the decay of the the $^2B_1(\pi_-)$ to the $^2B_1(\sigma)$ state on the B3LYP/6–31G* surface ($\Delta E = 0.85$ kcal mol^{-1}, -0.71 kcal mol^{-1} after inclusion of the ZPE difference). Given this result, we can safely neglect the $^2B_1(\pi_-)$ state as a candidate for the ground state of *syn*-**TOD**$^{\bullet+}$. Since the distorted $^2B_1(\sigma)$ and the $^2A_1(\pi_+)$ state are of the same symmetry in C_s, their interconversion was also examined. Thereby a very low-lying saddle point for this

0947-6539/00/0605-0862 $ 17.50+.50/0 *Chem. Eur. J.* **2000**, *6*, No. 5

"electromerization" was found on the B3LYP potential energy surface where it lies only 0.43 kcal mol^{-1} above the localized ^{2}A′(σ) state. After correcting for the ZPE difference, the activation energy for this process drops to nearly zero, so that, on the B3LYP surface, the σ-state is unstable with regard to decay to the $^2A_1(\pi_+)$ state. The situation is reversed at the CCSD(T) level where the $^2B_1(\sigma)$ is 2 kcal mol^{-1} more stable than the $^2A_1(\pi_+)$ state. The CCSD(T) energy of the B3LYP transition state lies also only 0.5 kcal mol^{-1} above the latter, but the reversed thermochemistry of this rearrangement at this level will lead to a change in the structure of the transition state, so this result may not be very meaningful. However, the above results suggest that both the $^2A_1(\pi_+)$ as well as the $^2B_1$ or the localized ^{2}A′(σ) states should be considered as possible ground states of *syn*-**TOD**$^{\bullet+}$.

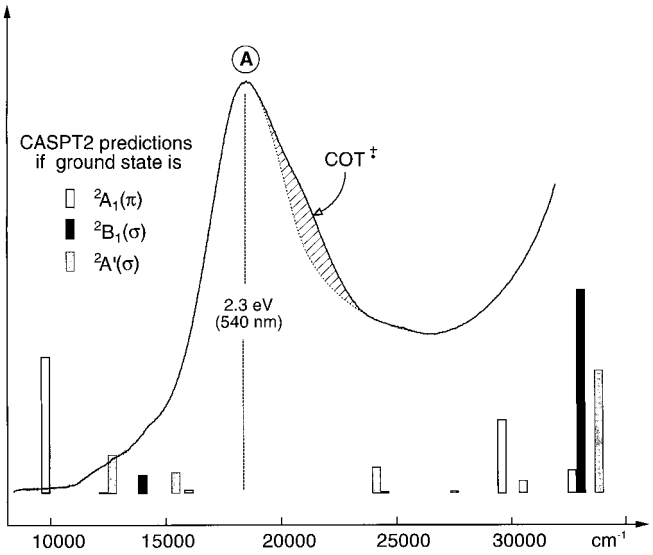

Figure 10. Spectrum a) from Figure 1 replotted on an energy scale, together with CASPT2 prediction of excitation energies and oscillator strengths for the different electromers of *syn*-**TOD**$^{\bullet+}$.

Figure 10 shows the spectrum of species **A** (redrawn on an energy scale) together with the CASPT2 predictions for the EA spectra of *syn*-**TOD**$^{\bullet+}$ in the $^2A_1(\pi_+)$, the $^2B_1(\sigma)$, and the distorted ^{2}A′(σ) states (cf. Table 2). Obviously, the experimental spectrum does not match even remotely with any of these predictions. In view of the fact that the CASPT2 method reproduced the excited state energies of *syn*-**TOD**$^{\bullet+}$ at the neutral geometry rather accurately (cf. PE spectrum in Figure 7), this result leads us to reject our initial hypothesis that the primary product observed on pulse radiolysis of *syn*-**TOD** is the parent radical cation. Consequently, we proceeded to explore possible low activation decay pathways of *syn*-**TOD**$^{\bullet+}$ in either of its possible ground states.

Table 2. Results of CASPT2 calculations for *syn*-**TOD**$^{\bullet+}$ in different states.[a]

State	Geometries[b] $^2A_1$[c]	$^2B_1(\sigma)$[c]	$^2A'(\sigma)$[c,d]	State
1^2A_1	(0)	1.73 (0.0123)	(0)	$1^2A'$
1^2B_1	1.21 (0.0816)	(0)	1.57 (0.0247)	$2^2A'$
2^2B_1	1.52 (0.0002)	2.05 (0.0001)	1.91 (0.0140)	$3^2A'$
1^2B_2	1.98 (0.0041)	3.97 (0)	2.99 (0.0168)	$1^2A''$
1^2A_2	2.47 (0)	4.26 (0.0001)	3.03 (0.0001)	$2^2A''$
2^2A_1	3.67 (0.0449)	4.10 (0.1202)	3.41 (0.0003)	$3^2A''$
2^2B_2	4.05 (0.0150)	4.27 (0)	4.14 (0.0000)	$4^2A''$

[a] Energies relative to ground state (0) in eV; details of the calculations are given in the Supporting Information; [b] geometries optimized by B3LYP/6–31G*; [c] numbers in parentheses are oscillator strenghts for electronic transitions from ground state; [d] 2B1(σ) state distorted to C_s symmetry; data in this column refer to state labels on the right.

Starting with the $^2B_1(\sigma)$ state, its distortion in the direction of **BOT**$^{\bullet+}$ seemed to indicate a possible decay to that species. However, the SOMO of *syn*-**TOD**$^{\bullet+}$ in the $^2B_1$ (or the distorted ^{2}A′) σ-state is symmetric, whereas the SOMO of ground state **BOT**$^{\bullet+}$ (^{2}A″) is antisymmetric with regard to the mirror plane common to the two isomers. Hence, the lowest σ-state of *syn*-**TOD**$^{\bullet+}$ correlates with an *excited* ^{2}A′ state of **BOT**$^{\bullet+}$. By means of linear synchronous transit (LST) calculations,[22] one can indeed map a diabatic C_s reaction pathway connecting these two states which are of similar energy. However, this pathway is of no practical significance, because the ^{2}A″ surface leading to the ground state of **BOT**$^{\bullet+}$ cuts through at an early stage. This will necessarily lead to a loss of symmetry ("uncrossing") to permit an adiabatic passage from the ^{2}A′ to the ^{2}A″ surface, as in the case of *anti*-**TOD**$^{\bullet+}$.[6]

In an effort to find the transition state for this process, we located the lowest energy crossing point of the A′ and A″ surfaces in C_s symmetry by state-averaged CASSCF calculations. Distortion at this point along an a″ mode with a negative frequency led to a transition state lying only 0.49 kcal mol^{-1} above the ^{2}A′(σ) state of *syn*-**TOD**$^{\bullet+}$ by B3LYP (0.32 kcal mol^{-1} after correcting for the ZPE difference). At the CCSD(T) level, the energy difference—this time relative to the more stable delocalized $^2B_1(\sigma)$ state—is 1.04 kcal mol^{-1}, still not enough to protect *syn*-**TOD**$^{\bullet+}$ in its σ-state from decay.

Surprisingly, B3LYP intrinsic reaction coordinate (IRC) calculations (see Figure 11) revealed that this transition state connects *syn*-**TOD**$^{\bullet+}$ *directly* to **COT**$^{\bullet+}$ without passing via the originally presumed primary product, **BOT**$^{\bullet+}$. This unexpected

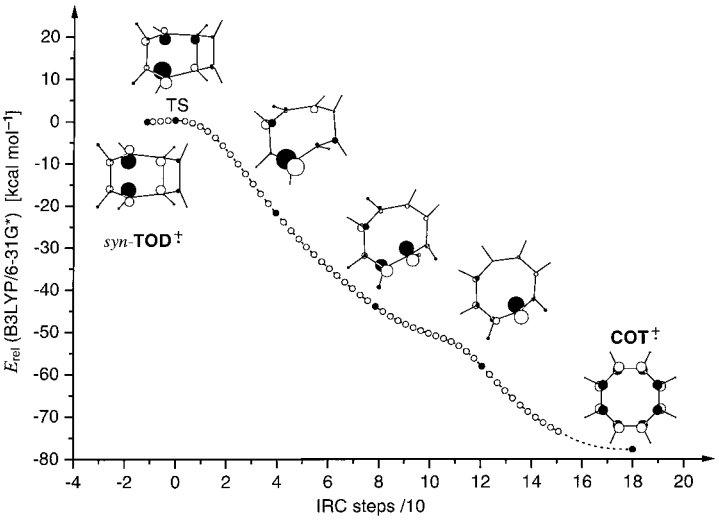

Figure 11. Results of IRC calculation for the ring-opening of *syn*-**TOD**$^{\bullet+}$ in the ^{2}A′ state. Note that this leads smoothly to **COT**$^{\bullet+}$, without passing through **BOT**$^{\bullet+}$. The singly occupied MO is shown for every filled dot.

result may, however, serve to explain the fact why **COT**$^{\bullet+}$ (rather than **BOT**$^{\bullet+}$) is formed as a primary product of ionization in all experiments, next to the hitherto unidentified species **A** and/or **B**. Apparently vertical ionization of *syn*-**TOD** results in a partitioning of the incipient radical cation between the $^2B_1(\sigma)$ and the $^2A_1(\pi_+)$ states, and the part which relaxes to the $^2B_1(\sigma)$ state decays spontaneously to **COT**$^{\bullet+}$.

Returning to the problem of identifying species **A**, we next examined the fate of the $^2A_1$ state of *syn*-**TOD**$^{\bullet+}$, that is the most stable state of that cation at the neutral geometry. Inspection of the B3LYP normal modes showed a framework deformation of b_2 symmetry with an unusually low frequency of 154 cm^{-1}. Following that mode led to a transition state only 0.05 kcal mol^{-1} above $^2A_1$ *syn*-**TOD**$^{\bullet+}$ which decayed on the far side by completely breaking a bond of the central four-membered ring to result in a bis-cyclobutenylium radical cation **BCB**$^{\bullet+}$. Actually, at the UHF or ROHF level, $^2A_1$ *syn*-**TOD**$^{\bullet+}$ is not a minimum but decays spontaneously to **BCB**$^{\bullet+}$, a feature which we had failed to notice due to our focus on DFT calculations as a starting point for all further investigations.

Bis-allylic radical cations such as **BCB**$^{\bullet+}$ are usually distinguished by broad and intense charge resonance (CR) bands[23] which arise by promotion of an electron from the bonding to the antibonding combination of the π-MOs, just as in sandwich dimer cations of π-systems[24] (cf. Figure 12). CASPT2 calculations at the B3LYP equilibrium geometry of **BCB**$^{\bullet+}$ (Table 3) predict indeed an intense band at 2.09 eV (590 nm), that is close to the strong band of species **A**. Note that the energy of this CR transition depends very critically on the overlap of the two π-systems which is dictated by the angle that the cyclobutenylium moieties form with the connecting bond (opening this angle up just 1.5° from the B3LYP optimized value would bring the transition into perfect accord with experiment). CASPT2 predicts no transitions of comparable intensity up to 250 nm (cf. Table 3), in accord with the observation of a single, strong CR band for species **A**. Thus, the different calculations concur in supporting an assigment of species **A** to **BCB**$^{\bullet+}$, which leaves the problem of assigning its thermal decay product **B**.

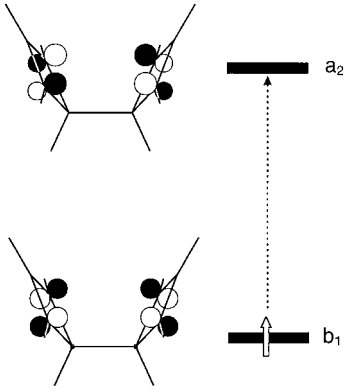

Figure 12. Pictorial representation of the $^2B_2 \rightarrow {}^2A_2$ charge resonance excitation in **BCB**$^{\bullet+}$.

Table 3. Results of CASPT2 calculations for **BCB**$^{\bullet+}$.[a]

State	EAS/ eV[b]	CASPT2/ eV[c]	f[d]
1^2B_1	(0)	(0)	–
1^2A_2	2.30	2.09	0.2221
1^2B_2		2.89	(0)
2^2A_2		3.50	0.0419
2^2B_2	(>4.0)	4.11	(0)
2^2B_1		4.72	<0.0001

[a] Geometry optimized by B3LYP/6–31G*; [b] band positions in electronic absorption spectrum, approximate for small bands (cf. Figure 13) in eV; [c] active space in CASSCF calculations: 13 electrons in 10 orbitals; details of the calculations are given in the Supporting Information; [d] calculated oscillator strength for electronic transition.

Assignment of the secondary product B: This species is formed in a single step from **A** and decays on warming above 80 K to **BOT**$^{\bullet+}$; hence **B** is most probably also a $(CH)_8$ isomer. Disrupting a four-membered ring of **BCB**$^{\bullet+}$ would call for the breaking of a strong C–C bond which would presumably require more energy than is available at 80 K. On the other hand, cyclobutenylium cations pucker spontaneously[25] and form partial transannular bonds to optimize the stabilizing interactions responsible for the pronounced homoaromatic character of these species.[26] In the case of **BCB**$^{\bullet+}$ this puckering is not spontaneous, because it disrupts the stabilizing interaction between the two cyclobutenylium moieties, but it certainly represents a low-energy distortion pathway leading to bicyclobutenyl structures. A search of different $(CH)_8$ species[1] turned up two compounds that might result from such a distortion, that is tetracyclo[4.2.0.0^{2,4}.0^{3,5}]oct-7-ene (**TCO**), and the bis(bicyclobutane) compound **BBB**. According to B3LYP calculations **TCO**$^{\bullet+}$ lies 6.3 kcal mol^{-1} below **BCB**$^{\bullet+}$, whereas **BBB**$^{\bullet+}$ is 1.9 kcal mol^{-1} less stable than **BCB**$^{\bullet+}$, so we focussed on **TCO**$^{\bullet+}$ as a possible candidate for **B**.

TCO **BBB**

CASPT2 calculations on **TCO**$^{\bullet+}$ at its B3LYP equilibrium geometry resulted in the predictions presented in Table 4 and Figure 13 which are in near-perfect accord with regard to the broad 820 nm band of species **B** and the absence of further intense absorptions in the visible region (the rise in the UV

Table 4. Results of CASPT2 calculations for **TCO**$^{\bullet+}$.[a]

State	EAS/ eV[b]	CASPT2/ eV[c]	f[d]
$1^2A'$	(0)	(0)	–
$2^2A'$	1.51	1.54	0.0953
$1^2A''$		2.38	0.0003
$3^2A'$	2.55	2.72	0.0051
$4^2A'$	3.20	3.41	0.0061
$2^2A''$		3.55	0.0071
$3^2A''$		4.11	0.0063
$4^2A''$	ca. 4 eV	4.23	0.0128

[a] Geometry optimized by B3LYP/6–31G*; [b] band positions in electronic absorption spectrum, approximate for small bands (cf. Figure 13) in eV; [c] active space in CASSCF calculations: 15 electrons in 13 orbitals; details of the calculations are given in the Supporting Information; [d] calculated oscillator strength for electronic transition.

0947-6539/00/0605-0864 $ 17.50+.50/0 *Chem. Eur. J.* **2000**, *6*, No. 5

may be due to a by-product that is formed in the course of the decay of **BCB**$^{\bullet+}$). Inspection of the CASSCF wavefunctions shows that the telling NIR transition of **TCO**$^{\bullet+}$ results from HOMO-1 →HOMO electron promotion, where both orbitals are linear combinations of cyclobutene π- and bicyclobutane σ-MOs (see Figure 13). The other weak transitions above 30000 cm^{-1} involve promotions from lower lying occupied MOs of **TCO**$^{\bullet+}$ to the HOMO, whereas only the higher excited states involve virtual MOs.

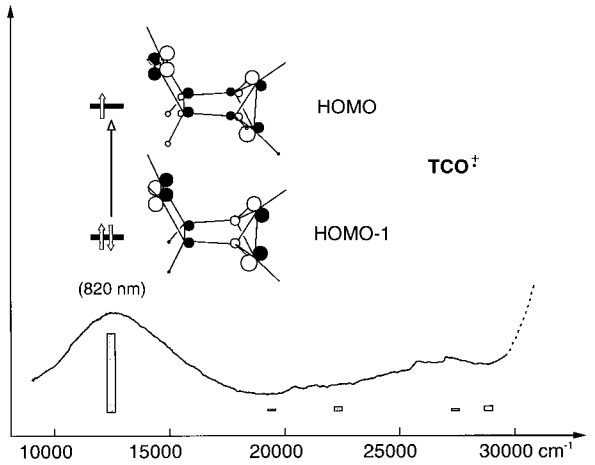

Figure 13. Spectrum B in Figure 5 replotted on an energy scale, together with CASPT2 prediction of excitation energies and oscillator strengths for **TCO**$^{\bullet+}$. The inset shows the MOs between which electron promotion occurs (predominantly) in the 820 nm transition.

In order to confirm this assignment, we synthesized **TCO**[27, 28] and subjected it to ionization by pulse radiolysis at 30 K in MCH. Indeed, a broad band at 820 nm was detected which exhibits the same thermal and photochemical behavior as species **B**. As an example, we show in Figure 14 the

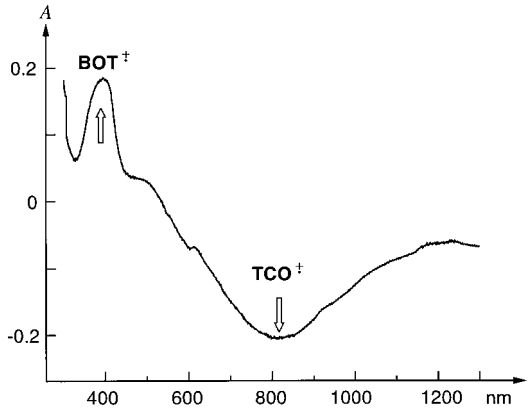

Figure 14. Difference spectrum for the photolysis at 950 nm (15 min) of an irradiated (pulse radiolysis) MCH/BuCl glass (30 K) containing **TCO**.

difference spectrum obtained on photolysis of **TCO**$^{\bullet+}$ which nicely demonstrates the conversion to **BOT**$^{\bullet+}$. We wish to recall at this point that this latter conversion occurs also thermally at temperatures above 77 K (cf. Figure 2) which raises the question of the mechanism for this rearrangement.

Returning to the ESR spectra in Figure 6, it is worth noting that the change on NIR photobleaching strongly suggests that the photoprecursor possesses an envelope spectrum extending over some 30–40 G in the center region. The identification of this species as **TCO**$^{\bullet+}$ is consistent with such an unresolved signal since the B3LYP calculations predict five different hyperfine couplings below 7 G for the 8 hydrogens with a total spectral width of only 40.8 G.

Vibronic coupling as a driving force for radical ion rearrangments: The assigments elaborated in the preceding sections imply that the $^2A_1(\pi_+)$ state of the radical cation of *syn*-**TOD** decays spontaneously to **BCB**$^{\bullet+}$ by breaking one of the "external" bonds in the central four-membered ring. In contrast, the *anti* isomer rearranges (partly) to **BOT**$^{\bullet+}$ by breaking one of the "internal" bonds in the same ring.[6] In view of the fact that the π-ground states of the two isomers are of very similar nature (see Scheme 1), the question arises what caused the two isomers to show such different intramolecular reactivity. Another, related question is why the $^2B_1(\sigma)$ state of *syn*-**TOD**$^{\bullet+}$ distorts so easily along the same mode as *anti*-**TOD**$^{\bullet+}$ (although the ensuing rearrangement seems to bypass **BOT**$^{\bullet+}$).

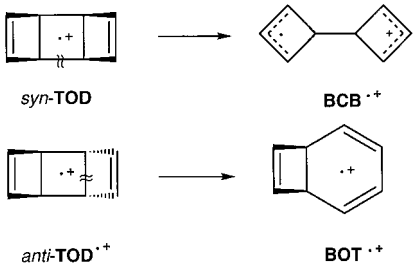

We believe that answers to these questions can be found by considering the effects of vibronic coupling which may be very important in shaping the potential energy surfaces of radical ions[29, 30] and in facilitating their rearrangements.[31, 32] If they are sufficiently strong, such effects can induce departure from a geometry of high symmetry as a result of the distortion along a coordinate q that allows the ground state Ψ_0 to mix with one or the other excited state Ψ_i of different symmetry.[33] The extent of this vibronic coupling is inversely proportional to the energy difference ΔE between Ψ_0 and Ψ_i and the force constant f_q for the deformation along q (both at the symmetric geometry where vibronic interaction is absent), and proportional to the derivative or nonadiabatic coupling term $V_{0i} = \langle \Psi_0 | \partial/\partial q | \Psi_i \rangle$ which measures the extent of mixing between Ψ_0 and Ψ_i on distortion along q.[34]

In the present case of *syn*-**TOD**$^{\bullet+}$ in its $^2A_1$ state, q must be of the same symmetry as Ψ_i to promote mixing with Ψ_0.[33] From the PE spectrum in Figure 7 we gather that, at the geometry of neutral *syn*-**TOD**, the lowest lying excited states Ψ_i are of B_1 symmetry (this appears to stay that way upon relaxation of the $^2A_1$ state to its equilibrium geometry, cf. Table 2). In view of the above mentioned ΔE dependence, one would therefore primarily expect b_1 modes to foster departure of *syn*-**TOD**$^{\bullet+}$ ($^2A_1$) from C_{2v} symmetry. However, the observed distortion (leading ultimately to **BCB**$^{\bullet+}$) is of b_2

symmetry, although, according to CASPT2, the lowest $^2B_2$ excited state of lies nearly 1 eV higher than the lowest $^2B_1$ state! Since the f_q for distortions of the central four-membered ring in *syn*-**TOD**$^{\bullet+}$ along b_1 and b_2 coordinates are probably quite similar, it must be owing to a larger coupling term V_{0i} that the $^2B_2$ state "wins" over the lower lying $^2B_1$ states in promoting distortion of *syn*-**TOD**$^{\bullet+}$($^2A_1$).

We have calculated the derivative coupling terms for the interaction of the $^2A_1$ with the two $^2B_1$ and with the $^2B_2$ excited states on distortion of each atom along the Cartesian axes. The resulting vectors (Figure 15) show that the largest V_{0i} is found for interaction with the $^2B_1(\pi_-)$ state which is induced by asymmetric stretching of the two double bonds. However, the

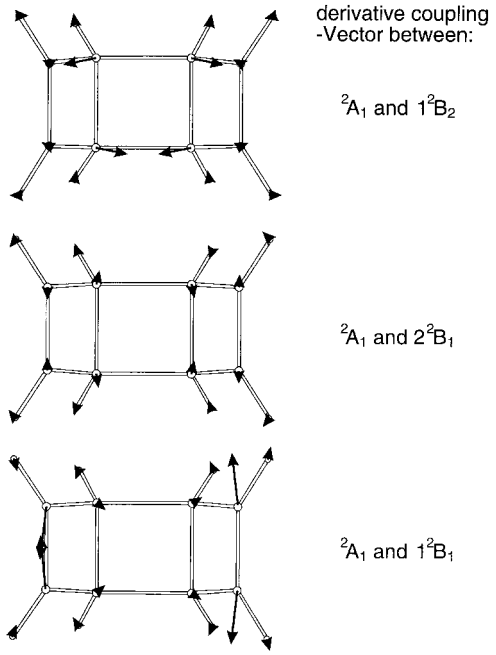

Figure 15. Derivative coupling vectors for the interaction of the $^2A_1(\pi_+)$ ground state of *syn*-**TOD**$^+$ with the $1^2B_1(\pi_-)$, the $2^2B_1(\sigma)$ and the $1^2B_2(\sigma)$ excited states (the arrows point in the direction of maximum change of the ground state wavefunction, i. e., maximum vibronic coupling).

force constant f_q for this deformation is too large to allow for a spontaneous distortion along this mode. The V_{0i} for interaction with the $^2B_1(\sigma)$ state is much weaker than for the interaction with the higher lying $^2B_2(\sigma)$ state, which may explain why the distortion along the b_2 mode "wins", and leads to the spontaneous decay of *syn*-**TOD**$^{\bullet+}$($^2A_1$) to **BCB**$^{\bullet+}$.

The facile distortion of *syn*-**TOD**$^{\bullet+}$ in its $^2B_1(\sigma)$ ground state, this time along a mode of b_1 symmetry, can be explained in the same fashion, that is through vibronic coupling to the (now excited) $^2A_1(\pi_+)$ state. An analogous effect seems to be operative in *anti*-**TOD**$^{\bullet+}$ which also distorts easily in the direction of **BOT**$^{\bullet+}$, and not **BCB**$^{\bullet+}$. A "chemical" reason for this preference might be, starting from *anti*-**TOD**$^{\bullet+}$, that **BCB**$^{\bullet+}$ arises in the *anti* conformation where it cannot profit from the stabilizing through-space interaction between the two allylic moieties. This makes the *anti*-**TOD**$^{\bullet+}$ $\rightarrow$**BCB**$^{\bullet+}$ reaction endothermic and thus deprives the corresponding distortion of a thermochemical driving force. Therefore, the other distortion, leading to **BOT**$^{\bullet+}$, becomes competitive.

Thus, the surprising departure of *syn*-**TOD**$^{\bullet+}$ from the least-motion pathway leading to **BOT**$^{\bullet+}$ is initiated by a strong vibronic coupling to the $^2B_2$ excited state which initiates the decay to **BCB**$^{\bullet+}$. The ensuing conversion of the latter to **TCO**$^{\bullet+}$ may also be facilitated by vibronic interaction between the $^2B_2$ ground state with the lowest $^2A_2$ excited state of **BCB**$^{\bullet+}$. This requires a distortion of b_1 symmetry which leads to a localization of spin and charge in opposite allyl moieties, a necessary prerequisite for the formation of **TCO**$^{\bullet+}$.

Figure 16 shows a summary of our calculations for the full rearrangement of $^2A_1$ *syn*-**TOD**$^{\bullet+}$ to **COT**$^{\bullet+}$. Although the numbers may be subject to some uncertainty, even at the CCSD(T) level, the general picture that emerges from these calculations is in accord with the experimental findings and therefore supports our mechanistic conclusions; thus, after a nearly activationless decay of $^2A_1$ *syn*-**TOD**$^{\bullet+}$ to **BCB**$^{\bullet+}$, the latter species rearranges in a process associated with an activation barrier of 6.6 kcal mol^{-1} to **TCO**$^{\bullet+}$ which in turn decays to **BOT**$^{\bullet+}$ via a barrier that is calculated to be about twice as high as the first one. **BOT**$^{\bullet+}$ is protected from decay to **COT**$^{\bullet+}$ by a much higher barrier which can certainly not be surmounted at cryogenic temperatures. Hence, the **COT**$^{\bullet+}$ which is observed immediately after ionization even at 30 K must arise via a different mechanism. The calculations illustrated in Figure 11 indicate that **COT**$^{\bullet+}$ is formed by nearly activationless decay of *syn*-**TOD**$^{\bullet+}$ in its $^2B_1$ (or $^2A'$) state.

Summary and Conclusion

We have shown by a combination of different types of experiments and quantum chemical calculations that upon ionization, *syn*-**TOD** partitions between two electronic states ($^2A_1$ and $^2B_2$) which decay to different products, both of which are formed within the duration of the 4 μs electron pulse at 30 K (see Scheme 2). Calculations indicate that **COT**$^{\bullet+}$ is formed in a nearly activationless process out of the $^2B_1$ state (perhaps after spontaneous relaxation of this state to C_s symmetry), whereas the $^2A_1$ state decays to the bis-allylic cation **BCB**$^{\bullet+}$. Upon warming of the matrix, the latter product rearranges to the tetracyclic isomer **TCO**$^{\bullet+}$ (the first product observed at 77 K) which on further warming to 90 K undergoes a bicyclobutane – butadiene rearrangement to yield the final product, **BOT**$^{\bullet+}$.

Both of the primary products are formed as a result of strong vibronic interactions which lead to spontaneous (or very facile) distortions that carry *syn*-**TOD** part of the way along the respective reaction coordinates. Interestingly, the excited states which lead to these distortions are not necessarily the lowest ones, but those which are associated with the largest derivative coupling terms. The present example shows very clearly that principles which govern rearrangements of neutral compounds, such as that of the least motion pathway, are not necessarily operative in radical ions. Instead, the reactivity of these species is often dominated

0947-6539/00/0605-0866 $ 17.50+.50/0 *Chem. Eur. J.* **2000**, *6*, No. 5

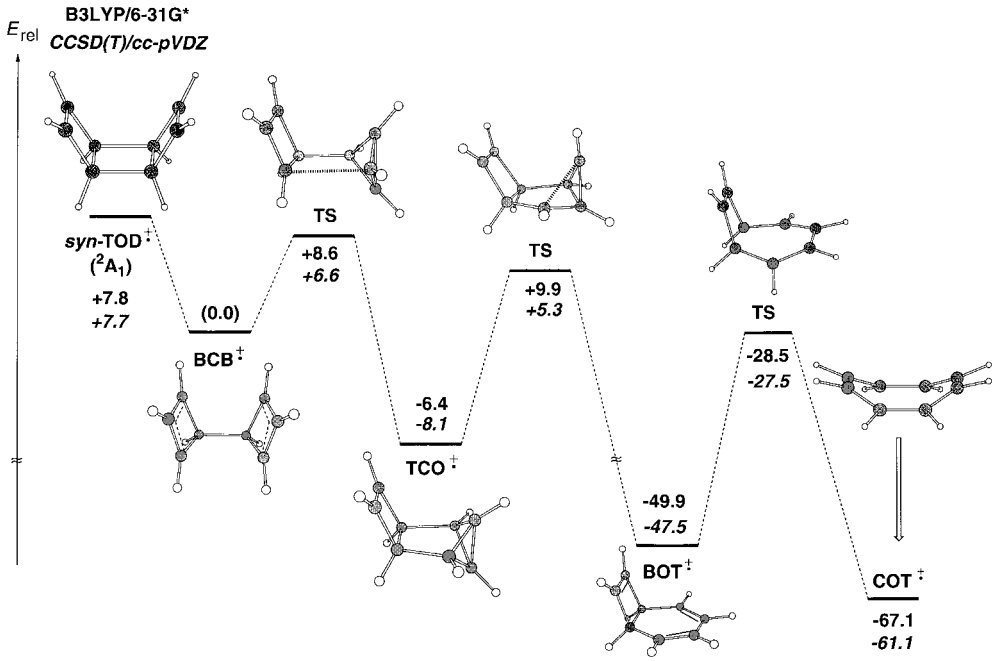

Figure 16. Schematic representation of the potential energy surface leading from $^2A_1$ *syn*-**TOD**$^{+\cdot}$ via **BCB**$^{+\cdot}$ and **TCO**$^{+\cdot}$ to **BOT**$^{+\cdot}$. Geometries obtained by B3LYP/6–31G*, single-point energies by CCSD(T)/cc-pVDZ include B3LYP zero point energies (italic numbers).

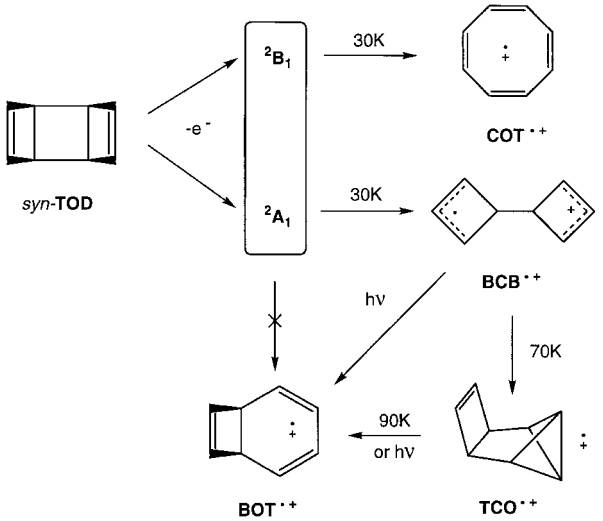

Scheme 2. Different radical ion rearrangements.

by effects of vibronic interaction which may be decisive in shaping the potential energy surfaces on which radical ion rearrangements take place.

Experimental Section

Synthesis: *syn*-Tricyclo[4.2.0.0^{2,5}]octa-3,7-diene (*syn*-**TOD**) was synthesized by dehalogenation of dichlorocyclobutene[35] (Fluka, purum) by Na amalgam which was prepared in situ. In the workup, the conversion to the silver complex[35] was replaced by purification by preparative gas chromatography at room temperature using β,β'-oxidiproprionitrile (ODP) as a stationary phase. The preparation of tetracyclo[4.2.0.0^{2,4}.0^{3,5}]oct-7-ene (**TCO**) followed the prescriptions of Meinwald et al.[27, 28] For the isolation of the product, pentane was added to the reaction mixture, THF and ether were removed by repeated aqueous extraction, the amine was removed by rapid extraction with 1M Na_2HPO_4 and the resulting solution was finally washed with aqueous ammonia.

Sample preparation: $\approx 5 \times 10^{-3}$M solutions of *syn*-**TOD** were prepared in $CFCl_2CFCl_2$ (F-112), CF_2ClCCl_3 (F-112a), $CF_2ClCFCl_2$ (F-113), CF_3CCl_3 (F-113a) for ESR measurements, or a 1:1 mixture of $CFCl_3$ (F-11) and CF_2BrCF_2Br (F-114B2),[36, 37] or 1M *n*-butyl chloride (BuCl) in methylcyclohexane (MCH) for optical studies. These solutions were filled into quartz tubes (ESR work) or special optical cuvettes,[38]where they were exposed to $\approx$0.5 MRad of ^{60}Co γ-radiation at 77 K.

Pulse radiolysis: The samples (2 mm thick) were mounted in a liquid helium-cooled cryostat (Oxford Instruments) and irradiated with 4 μs electron pulses (delivering a dose $\approx$1 kGy) from ELU-6 linear accelerator. Details of the pulse radiolysis system are given elsewhere.[39]

Spectroscopy: All ESR measurements were carried out on a Bruker ER 200 D SRC spectrometer (TE_{102} cavity, ER-4102-ST X-band resonator, 35 dB microwave power) equipped with variable-temperature accessories. The PE spectrum of *syn*-**TOD** was recorded on a modified Perkin–Elmer PE 16 instrument operated in preretardation (and hence constant resolution) mode[40] under computer control. Calibration was effected with a Xe/Ar mixture and the spectral resolution was about 12 meV (digital resolution 2 meV). Electronic absorption (EA) spectra were measured on a Perkin–Elmer Lambda 19 (200–2000 nm), Philips 8710 (200–900 nm) and Cary 5 (Varian, 200–3300 nm) instruments.

Quantum chemical calculations: The geometries of all species were optimized at the UHF and UMP2 level as well as by methods based on density functional theory (DFT). For the latter we used Becke's 3-parameter (B3) exchange functional[41], combined with the Lee–Yang–Parr correlation functional[42] to give the B3LYP method[43] as implemented in the Gaussian 94 package of programs.[44] The above calculations were all done with the standard 6–31G* basis set. Except where otherwise indicated, stationary points were identified at all levels by Hessian calculations. In addition, transition states were characterized by full intrinsic reaction coordinate (IRC) calculations[45] to identify the minima they interconnect. Finally, single-point calculations were carried out on stationary points (usually at the B3LYP geometries) by the RCCSD(T) method[46] with Dunning's correlation-consistent polarized double-zeta basis set (cc-pVDZ),[47] using the MOLPRO program.[48]

For excited states we resorted to the CASSCF/CASPT2 procedure[49] with the MOLCAS program.[50] The active spaces were chosen such that they allowed all excited states that were considered in each case to be described satisfactorily according to the different diagnostic criteria given by the

MOLCAS program (similar weight of CASSCF in CASPT2 wavefunction for all states, absence of intruder states). As in previous cases of radical cations,[51–53] satisfactory agreement with experiment was obtained with the simple [C]3s2p1d/[H]2s ANO DZ basis set,[54] therefore we saw no necessity to add higher angular momentum and/or diffuse functions. Molecular orbitals were plotted with the Moplot program[55] which gives a schematic representation of the MOs nodal structures in a ZDO-type approximation.[56]

The derivative (or nonadiabatic) coupling terms discussed in the section on vibronic coupling were calculated by using a locally modified version of the for localizing conical intersection (opt=conical) of the Gaussian program.[57]

Acknowledgment

This work is part of project No. 2000-053568.98 of the Swiss National Science Foundation and Grant No. 3T09A11809 of the Polish State Committee for Scientific Research. The research of the Knoxville Group was supported by the Division of Chemical Sciences, Office of Basic Energy Sciences, U.S. Department of Energy, under Grant No. DE-FG02–88ER13852.

[1] K. Hassenrück, H.-D. Martin, R. Walsh, *Chem. Rev.* **1989**, *89*, 1125.
[2] S. Dai, J. T. Wang, F. Williams, *J. Am. Chem. Soc.* **1990**, *112*, 2835, 2837.
[3] T. Bally, L. Truttmann, S. Dai, J. T. Wang, F. Williams, *Chem. Phys. Lett.* **1993**, *212*, 141.
[4] T. Bally, L. Truttmann, S. Dai, F. Williams, *J. Am. Chem. Soc.* **1995**, *117*, 7916.
[5] T. Bally, L. Truttmann, J. T. Wang, F. Williams, *J. Am. Chem. Soc.* **1995**, *117*, 7923.
[6] T. Bally, S. Bernhard, S. Matzinger, L. Truttmann, Z. Zhu, J.-L. Roulin, A. Marcinek, J. Gebicki, F. Williams, G.-F. Chen, H. D. Roth, T. Herbertz, *Chem. Eur. J.* **2000**, *6*, 849.
[7] R. Gleiter, *Top. Curr. Chem.* **1979**, *86*, 197.
[8] A. Plonka, *Annu. Rep. Prog. Chem.* **1989**, *85*, 47.
[9] A. Marcinek, J. Gebicki, A. Plonka, *J. Phys. Org. Chem.* **1990**, *3*, 757.
[10] T. Bally, K. Roth, R. Straub, *Helv. Chim. Acta* **1989**, *72*, 73.
[11] T. Bally, S. Nitsche, K. Roth, E. Haselbach, *J. Am. Chem. Soc.* **1984**, *106*, 3927.
[12] G. Bieri, F. Burger, E. Heilbronner, J. P. Maier, *Helv. Chim. Acta* **1977**, *60*, 2213.
[13] S. Dai, J. T. Wang, F. Williams, *J. Am. Chem. Soc.* **1990**, *112*, 2835.
[14] S. Dai, J. T. Wang, F. Williams, *J. Am. Chem. Soc.* **1990**, *112*, 2837.
[15] R. Gleiter, E. Heilbronner, M. Hekman, H. D. Martin, *Chem. Ber.* **1973**, *106*, 28.
[16] N. Bodor, B. H. Chen, S. D. Worley, *J. Electron Spectrosc. Relat. Phenom.* **1974**, *4*, 65.
[17] G. Wipff, PhD thesis, Université Louis Pasteur, Strasbourg, **1971**.
[18] J. Spanget-Larsen, R. Gleiter, L. A. Paquette, M. J. Carmody, C. R. Degenhardt, *Theor. Chim. Acta* **1978**, *50*, 145.
[19] The optimzation of the $^2B_1(\pi_-)$ state was first carried out at the CASSCF level. At the resulting minimum, this state was the ground state and could be reoptimized by the B3LYP method.
[20] This is rather surprising in view of the known reluctance of DFT to localize spin and charge (or to overstabilize delocalized states). T. Bally, G. N. Sastry, *J. Phys. Chem. A.* **1997**, *101*, 7923.
[21] Y. K. Zhang, W. T. Yang, *J. Chem. Phys.* **1998**, *109*, 2604.
[22] T. A. Halgren, W. N. Lipscomb, *Chem. Phys. Lett.* **1977**, *49*, 225.
[23] B. Badger, B. Brocklehurst, *Trans. Farad. Soc.* **1970**, *66*, 2939.
[24] B. Badger, B. Brocklehurst, *Trans. Farad. Soc.* **1969**, *65*, 2576, 2582, 2588.
[25] G. A. Olah, J. S. Staral, R. J. Spear, G. Liang, *J. Am. Chem. Soc.* **1975**, *97*, 5489.
[26] S. Sieber, P. von R. Schleyer, A. H. Otto, J. Gauss, F. Reichel, D. Cremer, *J. Phys. Org. Chem.* **1993**, *6*, 445.
[27] G. E. Gream, L. R. Smith, J. Meinwald, *J. Org. Chem.* **1974**, *39*, 3461.
[28] L. R. Smith, G. E. Gream, J. Meinwald, *J. Org. Chem.* **1977**, *42*, 927.
[29] See e. g.: G. N. Sastry, T. Bally, V. Hrouda, P. Carsky, *J. Am. Chem. Soc.* **1998**, *120*, 9323.
[30] T. Bally, W. T. Borden in *Rev. Comput. Chem.*, *Vol. 13* (Eds.: K. B. Lipkowitz, D. B. Boyd), WILEY-VCH, New York, **1999**, pp. 1.
[31] F. Williams, *Acc. Chem. Res.* **1999**, to be submitted.
[32] I. B. Bersuker, *Electronic Structure and Properties of Transition Metal Compounds*, Wiley, New York, **1996**.
[33] The symmetry of a distortion q which leads to a mixing of Ψ_0 and Ψ_i is given by the direct product of the irreducible representations of the two state's symmetries: $\Gamma(q) = \Gamma(\Psi_0) \times \Gamma(\Psi_i)$.
[34] See, e. g.: H. Köppel, L. S. Cederbaum, W. Domcke, S. S. Shaik, *Angew. Chem.* **1983**, *95*, 211; *Angew. Chem. Intl. Ed. Engl.* **1983**, *22*, 210.
[35] M. Avram, I. G. Dinulescu, E. Marcia, G. Meteescu, E. Sliam, C. D. Nenitzescu, *Chem. Ber.* **1964**, *97*, 382.
[36] C. Sandorfy, *Can. J. Spectrosc.* **1965**, *85*, 10.
[37] A. Grimison, G. A. Simpson, *J. Phys. Chem.* **1968**, *72*, 1776.
[38] T. Bally in *Radical Ionic Systems*, *Vol. 6* (Eds.: A. Lund, M. Shiotani), Kluwer, Dordrecht, **1991**, pp. 3–54.
[39] S. Karolczak, K. Hodyr, R. Lubis, J. Kroh, *Radioanal. Nucl. Chem.* **1986**, *101*, 177.
[40] R. Dressler, L. Neuhaus, M. Allan, *J. Electron Spectrosc. Relat. Phenom.* **1983**, *31*, 181.
[41] A. D. Becke, *J. Chem. Phys.* **1993**, *98*, 5648.
[42] C. Lee, W. Yang, R. G. Parr, *Phys. Rev. B* **1988**, *37*, 785.
[43] B. G. Johnson, P. M. W. Gill, J. A. Pople, *J. Chem. Phys.* **1993**, *98*, 5612.
[44] M. J. Frisch, G. W. Trucks, H. B. Schlegel, P. M. W. Gill, B. G. Johnson, M. A. Robb, J. R. Cheeseman, T. Keith, G. A. Petersson, J. A. Montogomery, K. Raghavachari, M. A. Al-Laham, V. G. Zakrzewski, J. V. Ortiz, J. B. Foresman, J. Cioslowski, B. B. Stefanov, A. Nanayakkara, M. Challacombe, C. Y. Peng, P. Y. Ayala, W. Chen, M. W. Wong, J. L. Andres, E. S. Repogle, R. Gomperts, R. L. Martin, D. J. Fox, J. S. Binkley, D. J. DeFrees, J. Baker, J. J. P. Stewart, M. Head-Gordon, M. C. Gonzales, J. A. Pople, Gaussian, Inc., Pittsburgh, PA, **1995**.
[45] C. Gonzales, H. B. Schlegel, *J. Chem. Phys.* **1989**, *90*, 2154.
[46] Coupled-cluster method with single and double excitations supplemented by a non-iterative estimation of the contributions of triple excitations, based on a spin-restricted HF zero-order wavefunction. P. J. Knowles, C. Hampel, H.-J. Werner, *J. Chem. Phys.* **1993**, *99*, 5219.
[47] D. E. Woon, T. H. Dunning, *J. Chem. Phys.* **1993**, *98*, 1358.
[48] J.-J. Werner, P. J. Knowles, J. Almlöf, R. D. Amos, M. J. O. Deegan, S. T. Elbert, C. Hampel, W. Meyer, K. Peterson, R. Pitzer, A. J. Stone, P. R. Taylor, R. Lindh, **1996**.
[49] K. Andersson, B. O. Roos in *Modern Electronic Structure Theory*, *Part 1*, *Vol. 2*, World Scientific Publ. Co., Singapore, **1995**, pp. 55.
[50] K. Andersson, M. R. A. Blomberg, M. P. Fülscher, V. Kellö, R. Lindh, P.-Å. Malmqvist, J. Noga, J. Olson, B. O. Roos, A. Sadlej, P. E. M. Siegbahn, M. Urban, P.-O. Widmark, MOLCAS 4, University of Lund, Sweden, **1994**.
[51] M. P. Fülscher, S. Matzinger, T. Bally, *Chem. Phys. Lett.* **1995**, *236*, 167.
[52] Z. Zhu, T. Bally, J. Wirz, M. Fülscher, *J. Chem. Soc. Perkin Trans. 2* **1998**, 1083.
[53] T. Bally, C. Carra, M. P. Fülscher, Z. Zhu, *J. Chem. Soc. Perkin Trans. 2* **1998**, 1759.
[54] P.-O. Widmark, P.-Å. Malmqvist, B. O. Roos, *Theor. Chim. Acta* **1990**, *77*, 291.
[55] T. Bally, B. Albrecht, S. Matzinger, M. G. Sastry, MOPLOT 3.2, University of Fribourg, **1997**.
[56] E. Haselbach, A. Schmelzer, *Helv. Chim. Acta* **1979**, *54*, 1299.
[57] In the distributed version of Gaussian 98, only the coupling between the ground state and the first excited state can be evaluated. Slight modifications of the program were necessary to extend this capability to encompass higher excited states. We wish to thank Prof. Michael Robb for guiding us in implementing these changes.

Received: May 22, 1999 [F1874]

  0947-6539/00/0605-0868 $ 17.50+.50/0